Evaluation of Intracranial Microvessel Visualization in Mouse and Dog Models by Using a New Rotating Cerium Anode X-ray System

Chiharu TANAKA[*1,2], Toru SHIZUMA[*1], Yoshiro SHINOZAKI[*1], Kikue TODOROKI[*1], Yoshimori IKEYA[*1], Naoto FUKUYAMA[*1], Toshihiko UEDA[*2] and Hidezo MORI[*1]

[*1]*Department of Physiology, Tokai University School of Medicine*
[*2]*Department of Cardiovascular Surgery, Tokai University School of Medicine*

(Received November 4, 2016; Accepted November 25, 2016)

Objective: Lacunar stroke may be caused by infarction of small perforating branches of the middle cerebral artery. We developed a microangiographic X-ray system using a cerium anode to evaluate the perforating branches.
Methods: Iodine has K-edges at 33.2 kilo electron volts. Cerium yields a characteristic X-ray of 34.6 kilo electron volts, therefore, the cerium anode X-ray system could detect tiny amounts of contrast material. First, an X-ray chart was used to evaluate the resolution. Second, the brains of mice were dissected and irradiated. Third, the brains of dogs were excluded and irradiated. Fourth, iodine was perfused into the carotid artery of living dogs during brain imaging.
Results: In the first experiment, the cerium anode X-ray system elicited 4.86 clear line pairs. In mice, the perforating branches of the middle cerebral artery could be visualized. The perforating branches were clearly observed in dog brains ex situ even through an acrylic plate, but not in conventional X-ray images. Iodine moving inside the perforating branches was visualized in dog brains in situ using the cerium anode X-ray system.
Conclusion: The cerium anode X-ray system allowed us to visualize the perforating branches of the middle cerebral artery in living dogs.

Key words: Cerebral angiography, Microvessels, A cerium anode

INTRODUCTION

Lacunar stroke is typically caused by the infarction of a single penetrating artery seated in the deep structures of the brain, or in the brainstem [1]. Lacunar stroke accounts for 20% to 25% of all ischemic strokes [2], and patients who have experienced a lacunar infarct frequently experience disruption to their daily lives and may subsequently develop dementia, a particular risk for elderly patients [3]. Motor dysfunction, one of the major symptoms of a lacunar stroke, is an important predictor of disease pathogenesis, wherein motor function deteriorates with infarct stage. In such situations, immediate diagnosis and treatment are required. However, the intracranial perforating branches of the middle cerebral artery (MCA), which are responsible for lacunar stroke, are difficult to evaluate using conventional X-ray imaging techniques due to their small diameter. Behrouz *et al*. indicated that small vessel cerebral disease on brain imaging is certainly helpful in predicting the risk of recurrence, however, an angiographic mechanism to definitively quantify the severity of small vessel cerebral disease does not exist. The future of small vessel infarct is depending on accurate prognostication and effective management [2]. Moreover, Bailey *et al*. indicated, from a pathological point of view, that the cause of infarction remains unclear, and microvascular changes were spread throughout the deep gray and white matter not just around a symptomatic lesion [4]. For the accurate diagnosis and the further understanding of the small vessel cerebral disease, the new device for visualizing microvessels is more expected.

In recent years, the cerium anode X-ray system has been developed for clinical use. Cerium anode X-ray technology features a stronger spatial resolution than conventional X-ray techniques, and may therefore be useful for the assessment of human intracranial microvesssels. In the current study, a series of four experiments were performed in order to determine the efficacy of the cerium anode X-ray system in visualizing the intracranial perforating branches of the MCA, with a focus on identifying a potentially novel diagnostic tool for the early intervention of small vessel cerebral disease.

MATERIALS AND METHODS

Ethical approval of all experiments was provided by the Ethical Committee of Tokai University School of Medicine (Kanagawa, Japan), on 20 April 2012, and 1 October 2012. Associated permit numbers are 121033, 121067, 121099, and 122002. The investigation confirms with The Guide for the Care and Use of Laboratory Animalspublished by the U.S. National Institutes of Health (NIH Publication No. 85−23, revised 1996).

Chiharu TANAKA, Department of Physiology, Tokai University School of Medicine, 143 Shimokasuya, Isehara, Kanagawa 259-1193, Japan
Tel: +81-463-93-1121 Fax: +81-463-93-1125 E-mail: chitty@is.icc.u-tokai.ac.jp

For mice and dogs breeding, the temperature was maintained at 23 ± 2°, and the humidity was also maintained at 50 ± 15%. Interior light was turned on and off every 12 hours. For mice, CE-2 (CLEA Japan, Inc., Tokyo, Japan) was fed ad libitum, chlorine water (10 ppm) was given. For dogs, DS-A (Oriental Yeast Co., Tokyo, Japan) was restrictively fed once a day, and water was fed by the automatic waterer thorough the aqua filter. The toys for dogs were given as needed.

Euthanasia was achieved by intraperitoneal administration of pentobarbital (200 mg/kg) in mice, and by intravenous injection of pentobarbital (75 mg/kg) in dogs.

Monochromatic X-ray system using a rotating cerium anode

A monochromatic X-ray system incorporating a rotating cerium anode was developed for the purpose of the present study. Fig. 1A displays the relationship between the mass attenuation coefficient and X-ray photon energy. Iodine and barium are widely used in clinical settings as contrast materials. The mass attenuation coefficient of iodine demonstrates a sudden spike at 33.2 kilo electron volts (keV) (Fig. 1A), and this property is referred to as the K-edge of iodine. The K-edge of barium is at 37.4 keV. As visible in Fig. 1 A, the difference in the mass attenuation coefficient between contrast materials and human body tissue creates what is known as an angiographic contrast. Notably, the photon energy of cerium which gives maximum photon number is just above the K-edge of iodine and around that of barium (as indicated in Fig. 1A). Therefore, using a cerium anode in a monochromatic X-ray system is advantageous for the detection of small amounts of contrast material [5–7]. The cerium anode yields a characteristic X-ray emission with peak energy at 34.6 keV and a narrow distribution from 20 to 50 keV, as shown in Fig. 1B.

The CMOS-Flat panel (Hamamatsu Photonics, Shizuoka, Japan), which demonstrates a high spatial resolution of 50 μm and a 12 cm^2 field of vision, was used as a detector. The cerium anode X-ray system was composed of relatively small instruments, as indicated by Fig. 1C.

Estimating the spatial resolution of the cerium anode X-ray system (Experiment 1)

Spatial resolution was assessed using an X-ray test chart. The chart was exposed using either the cerium anode or a conventional tungsten anode X-ray system (Radiotex Safire R-30H, Shimadzu Corporation, Kyoto, Japan). The energy of the cerium anode X-ray was adjusted by voltage, current, and exposure time within the limits of 60–100 kV, 50–100 mA, and 100–1000 ms, respectively. Irradiation was conducted in three ways: directly, or indirectly by the insertion of either a 10- or 20-cm-thick acrylic plate between the device and the imaged object. The acrylic plate was used to substitute the thickness of the human body, 10 cm for children and 20 cm for adults.

Dosimetry data was obtained for the cerium anode X-ray system using a dosimeter at a voltage of 80 and 100 kV, an electrical current of 50 mA, exposure time of 100 ms, and a focal distance of 50 cm. Dosimetry analysis was performed 10 times, and the values across trials were averaged. Dosimetry data at 80 kV were also acquired at a longer exposure time of 1000 ms.

Mouse models (Experiment 2)

Severe combined immunodeficiency (SCID) mice were experienced, because we compared vasculature of the intracranial vessels with previous report which used SCID mice [8]. Thirty-two mice (age, 10 weeks old; average weight, 30 g; CLEA Japan, Tokyo, Japan) were anesthetized with isoflurane (2–2.5%). Barium contrast material (Barytgen, Fushimi Pharmaceutical Co., Kagawa, Japan) was filtered through a 10 μm mesh, concentrated by centrifugation, and injected directly into the left ventricle of the heart of anesthetized mice in order to fulfill the intracranial arteries. Barium contrast material was selected for this ex-situ experiment, as barium could stay in the vascular beds for a certain period in the excised brain, enabling the microangiography of the excised brain. By contrast, commercially available iodine contrast materials disperse immediately after the injection. Following the injection of pentobarbital (200 mg/kg) into the abdominal cavity, the brains were extracted and stored in formalin. One week after the operation, the excised brains were imaged using the cerium anode X-ray system.

Ex-situ dog models (Experiment 3.1)

Three beagle dogs (male; age, 27 months old; average weight, 10 kg; Kitayama Labes, Nagano, Japan) were anesthetized via injection of midazolam (0.4 mg/kg), dexmedetomidine (20 μg/kg), and butorphanol (0.3 mg/kg) as the bolus infusion, and propofol (6 mg/kg/h) via an intravenous line to maintain anesthesia during the operation. The beagles were then intubated. Following thoracotomy in the third intercostal space, the descending aorta and the subclavian artery were clamped. Filtered and concentrated barium (by the same procedure as above) was injected directly into the ascending aorta using a needle directed toward the intracranial arteries. The intracranial arteries were then filled with barium until they turned white, and pentobarbital (150 mg/kg) was then injected into the intravenous line. Barium contrast material was used for the reason stated above. The brains were then extracted and stored in formalin. A week later, the brains were exposed to both the cerium anode and conventional X-ray systems (using the same procedure as above), so that image quality could be compared. The excised brains were directly irradiated using the cerium anode X-ray system from 80 to 100 kV, at 50 mA for 100 ms and at a focal distance of 50 cm. Using the conventional X-ray system, the brains were irradiated at 60 kV for 6.3 milliampere-seconds, and at a focal distance of 50 cm. Furthermore, ex-situ angiography was repeated using 10 and 20 cm acrylic plates for both X-ray systems. With the acrylic plates, radiation from the cerium anode X-ray system was voltage-adjusted from 60 to 100 kV, and current-adjusted from 50 to 80 mA. The exposure time for these conditions was fixed at 1000 ms, and the focal distance was set to 50 cm. The same brain was then exposed using the conventional X-ray system in virtually equivalent con-

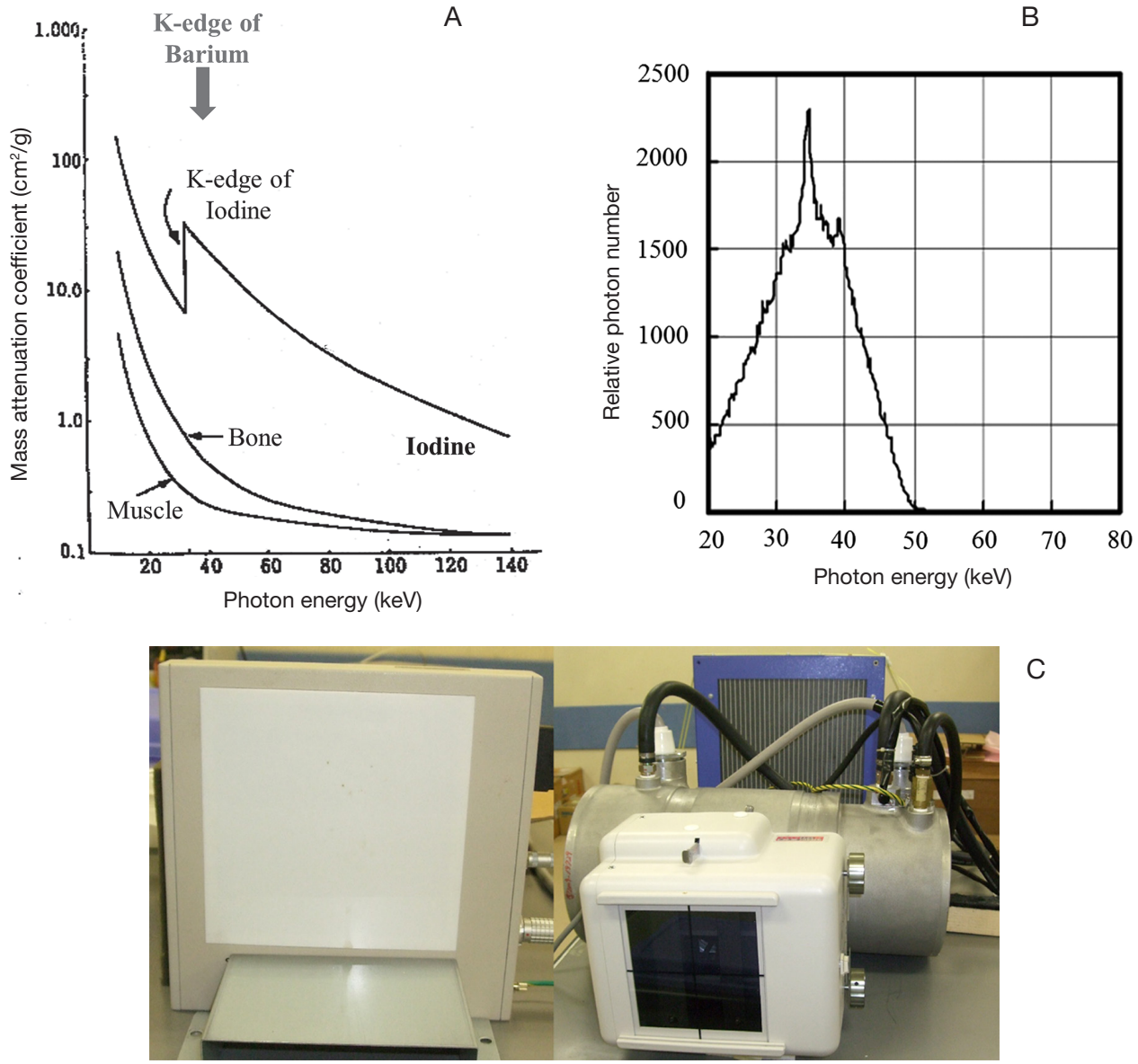

Fig. 1 A) Relationship between the mass attenuation coefficient and the X-ray photon energy. The difference in the mass attenuation coefficient between contrast materials and human body tissue creates angiographic contrast. The mass attenuation coefficient is comprised of a sudden rise in photon energy, called the K-edge, which is 33.2 keV and 37.4 keV for iodine and barium, respectively. Therefore, the angiographic contrast will be maximal at the K-edge of the contrast materials.
B) The X-ray spectrum as measured by the cerium anode X-ray system. The peak energy of the spectrum was identified at 34.6 keV, which is above the K-edge of iodine and barium.
C) The cerium anode X-ray system. The system consisted of a generator with a high heat unit (right), and a detector with high spatial resolution (left).

ditions, with the voltage ranging from 60 to 100 kV, milliampere-seconds from 6.3 to 8.0, and a distance of 50 cm.

In situ dog models (Experiment 3.2)

Two beagles (male; age, 27 months old; average weight, 10 kg; Kitayama Labes, Nagano, Japan) were anesthetized using a bolus infusion of midazolam (0.4 mg/kg), dexmedetomidine (20 μg/kg), and butorphanol (0.3 mg/kg), followed by injection of propofol (6 mg/kg/h) through an intravenous line to maintain anesthesia during the operation. The dogs were then intubated, and the left external carotid artery was catheterized toward the common carotid artery so that the iodine contrast materials (Iomeron 400, Eisai Global, Tokyo, Japan) could be perfused into the intracranial arteries via the blood flow from the heart. The head of each dog was then fixed in front of the detector and irradiated for 5 seconds during iodine perfusion. Images were taken using the cerium anode X-ray system at half-second intervals for 5 seconds, using voltage from 60 to 90 kV, electrical currents from 70 to 90 mA, and at a focal distance of 70 cm. Approximately 10 ml of iodine was injected into the intravenous line during the exposure.

Images of the same brain were also obtained by CT scan (SOMATOM Definition Flash, Siemens Global, Munich, Germany) using an iodine injection (same

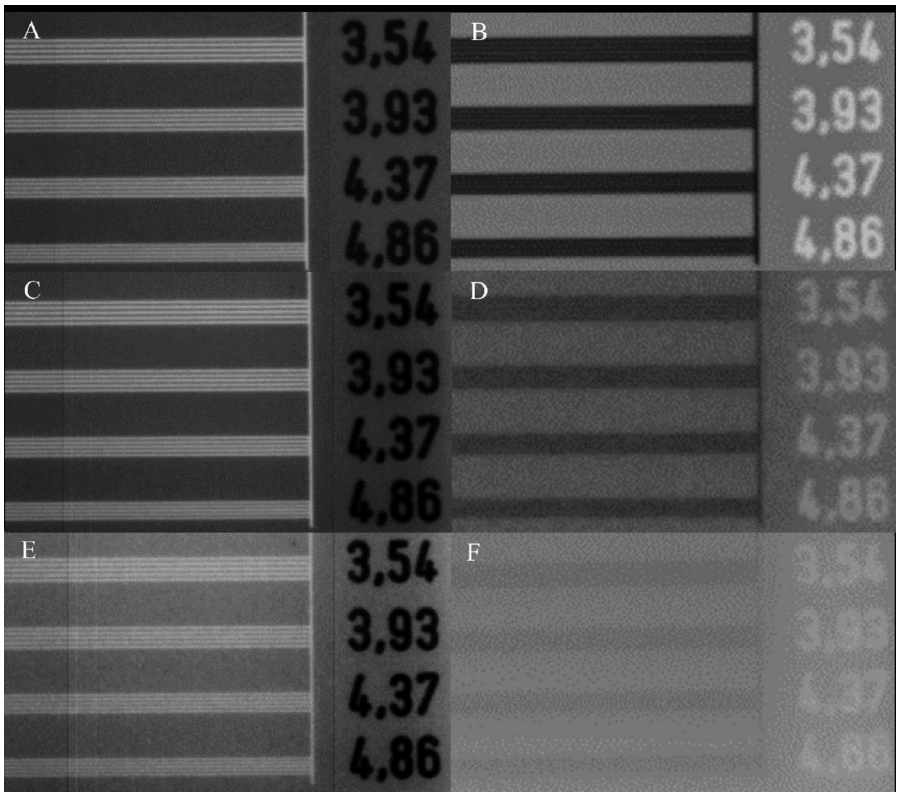

Fig. 2 X-ray test chart following various types of X-ray system exposure:
A) Direct exposure to the cerium anode X-ray system.
B) Direct exposure to the conventional X-ray system.
C) Indirect exposure to the cerium anode X-ray system through a 10-cm-thick acrylic plate.
D) Indirect exposure to the conventional X-ray system through a 10-cm-thick acrylic plate.
E) Indirect exposure to the cerium anode X-ray system through a 20-cm-thick acrylic plate.
F) X-ray test chart after indirect exposure to the conventional X-ray system through a 20-cm-thick acrylic plate.

procedure as above). Following the administration of pentobarbital (150 mg/kg) into the intravenous line, the brain was filled with concentrated barium and removed. Finally, the brain was irradiated using the cerium anode X-ray system to confirm the site of the perforating branches.

RESULTS

Evaluation of spatial resolution using the X-ray test chart (Experiment 1)

Images of the X-ray chart generated by exposure to the cerium anode X-ray system distinguished 4.86 line pairs/mm (calculated distance of the line pair, 103 μm) or more (Fig. 2A). As displayed in Fig. 2B, the conventional X-ray system did not clearly distinguish 4.86 line pairs/mm and featured heavy blurring. Using the 10- and 20-cm-thick acrylic plates, 4.86 line pairs/mm were still sufficiently visible for the evaluation by the cerium anode X-ray system (Figs. 2C and 2E). By contrast, using the conventional X-ray system, it was difficult to distinguish the lines at 3.54 line pairs /mm (calculated distance of the line pair, 141 μm) with the 10-cm-thick acrylic plate, as indicated in Fig. 2D. Additionally, with the 20-cm-thick acrylic plate, the lines in 3.54 line pairs/mm were barely distinguishable by the conventional X-ray system (Fig. 2F).

The dosimetry values of the cerium anode X-ray system under 100 ms of irradiation were 0.032 mGy at 80 kV and 50 mA, and 0.057 mGy at 100 kV and 50 mA. For 1000 ms, the dosimetry value was 5.342 mGy at 80 kV and 50 mA.

Brain images in mice (Experiment 2)

Fig. 3 displays brain images in mice that were irradiated with 90 kV at 50 mA for 100 ms by the cerium anode X-ray system. The focal distance from the cerium anode to the center of the brain was 30 cm. The wire, which was 100 μm in diameter, was used as a measuring scale (Fig. 3A).

The Circle of Willis was clearly visible, as indicated by the white arrowheads in Fig. 3A, and measured approximately 100 μm in diameter. Several cortical branches were visualized penetrating from the surface toward the cerebral cortex (black arrowheads, Fig. 3B). The perforating branches of the MCA could also be visualized, as indicated by the white arrowheads in Fig. 3C. The diameter of the cortical branches and the perforating branches was around 50 μm.

Brain images in ex-situ dogs (Experiment 3.1)

An example of an excised brain is displayed in Fig. 4A; the arterial system turned white when filled with barium. Ex-situ cerebral angiograms as imaged by the cerium anode X-ray system are presented in Figs. 4B (lateral position) and 4D (frontal position) with no acrylic plate, Fig. 4F with a 10-cm-thick acrylic plate, and Fig. 4H with a 20-cm-thick acrylic plate.

The perforating branches of the MCA were clearly

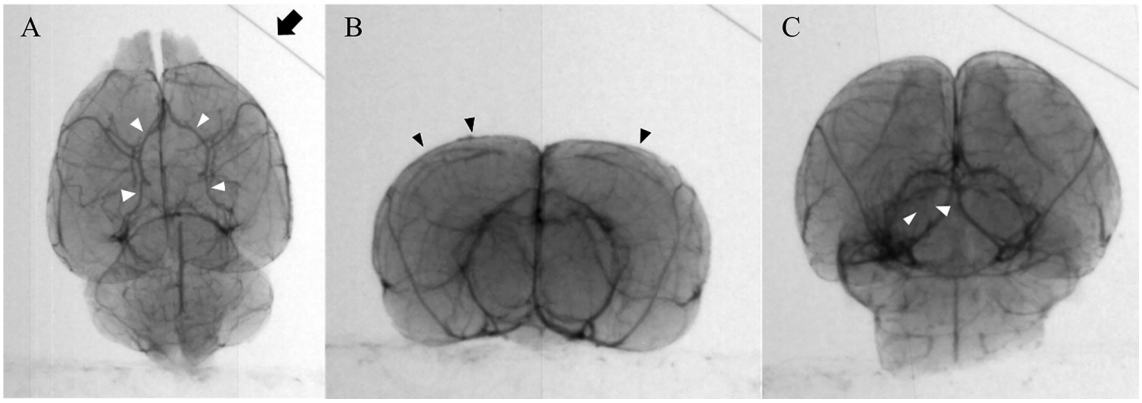

Fig. 3 Images of mouse brains as generated by the cerium anode X-ray system. The diameter of the vessels was calculated using a 100-μm wire, as indicated by the black arrow in Fig. 3A. The Circle of Willis, cortical branches, and perforating branches of the MCA are indicated by the arrowheads in Figs. 3A, 3B, and 3C, respectively.

visualized in the absence of the acrylic plate, as indicated by the white arrowheads in Figs. 4B and 4D. The perforating branches were visualized, running from the MCA in the direction of the posterosuperior region (Fig. 4B). The diameter of the arteries was determined to be less than 100 μm. By contrast, the conventional X-ray system did not clearly visualize the perforating branches in the same brain, as indicated by the black arrowheads in Figs. 4C and 4E. Using 10- (Fig. 4F) and 20-cm-thick acrylic plates (Fig. 4H), the perforating branches of the MCA (white arrowheads) were better visualized by the cerium anode X-ray system. Alternatively, the branches were barely visualized when irradiation was carried out using the conventional X-ray system with the 10 (Fig. 4G) and 20-cm-thick acrylic plates (Fig. 4I).

Moving image of in-situ dog models (Experiment 3.2)

The real-time angiography of in-situ dog models also demonstrated that iodine inside the perforating branches of the MCA could be clearly visualized, wherein the movement of the iodine was apparent during irradiation (white arrowheads, Fig. 5. the moving image is not shown). In another experiment, the perforating branches of the MCA were similarly visualized. In a CT scan that was done immediately after the cerium anode X-ray angiography in the same dog (Fig. 5), the perforating branches were barely visible (white arrowheads, Fig. 6).

DISCUSSION

The present study demonstrated that a rotating cerium anode X-ray system could clearly separate 4.86 line pairs/mm (spatial resolution of equal or less than 103 μm, Fig. 2) in an in-vitro experiment, visualize perforating branches originating from the MCA in an ex-situ experiment using both mice (Fig. 3) and dogs (Fig. 4), and in-vivo canine experiments (Fig. 5). Such results suggest a possible application for the current system in clinical settings in the near future.

Microangiographic X-ray system using a rotating cerium anode

In the current study, a new X-ray system was developed using a rotating cerium anode, which was capable of detecting small amounts of contrast material. Tungsten, which is widely used as an anode for conventional X-ray systems, features its highest energy at 69.5 keV and a wide distribution of between 10 to 140 keV. The K-edge values of the contrast materials are not close to the highest energy values of the conventional X-ray system using a tungsten anode; therefore, the conventional X-ray system is difficult to visualize small vessels. Subsequently, the X-ray system using a cerium anode with an energy peak of 34.6 keV is more suitable for the visualization of small vessels than the conventional X-ray system with a tungsten anode.

The X-ray generator of the cerium anode X-ray system features a high heat capacity (5 mega heat units) without the use of a metallic filter. Consequently, the X-ray system is able to maintain sufficient photon numbers after passing through the skin, muscles, and bones. The cerium anode was designed to rotate constantly to dissipate heat, as the cerium itself is not heat tolerant.

The ability of the visualization by the cerium anode X-ray system

The cerium anode X-ray system was able to visualize vessels as small as 50 μm, which is the limit of the detector of the cerium anode X-ray system (experiment 2). Perforating branches from the MCA were visualized in the canine ex-situ model using the cerium anode X-ray system, even in the presence of an acrylic plate (experiment 3.1). The perforating branches were smaller in canine models than humans; therefore, the branches would likely be more clearly visualized if used clinically. Additionally, the living dogs were exposed by the cerium anode X-ray system to enhance the perforating branches inside the skull (experiment 3.2). This experiment was performed in a preclinical style, in order to analyze the functional efficacy of the cerium anode X-ray system. The canine perforating branches were visualized in-situ, suggesting that the cerium anode X-ray system would sufficiently detect real-time blood flow inside the perforating branches in the human body. Conversely, a CT scan of the same brain was not able to depict the perforating branches. Therefore, the cerium anode X-ray system demon-

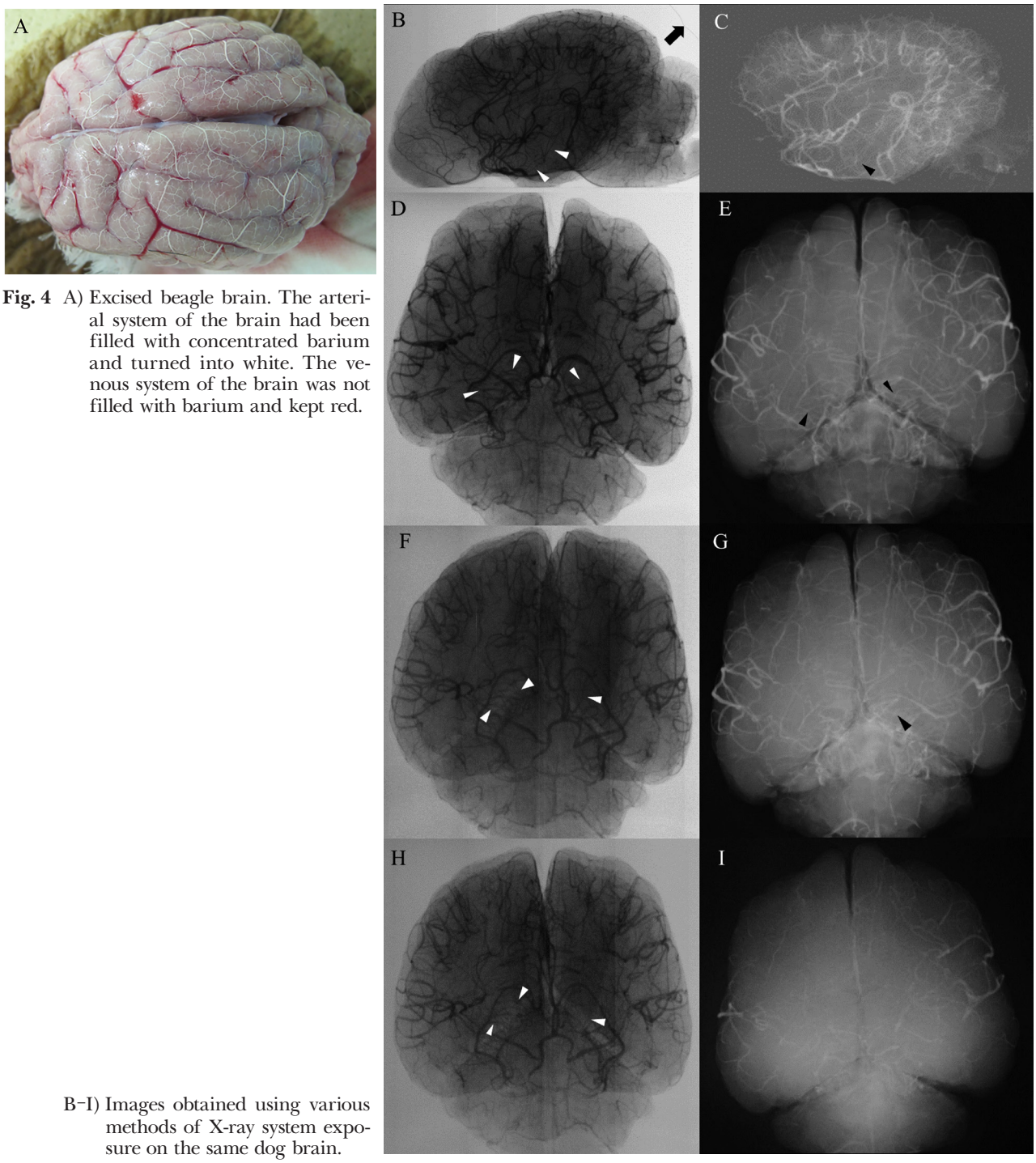

Fig. 4 A) Excised beagle brain. The arterial system of the brain had been filled with concentrated barium and turned into white. The venous system of the brain was not filled with barium and kept red.

B–I) Images obtained using various methods of X-ray system exposure on the same dog brain.

B) Sagittal brain image, acquired by the cerium anode X-ray system. The perforating branches of the MCA are clearly shown, as indicated by the white arrowheads.

C) Sagittal brain image, acquired by the conventional X-ray system. Branches are visualized but blurred, as indicated by the black arrowhead.

D) Coronal brain image, acquired via direct exposure to the cerium anode X-ray system. The perforating branches of the MCA are clearly visualized, as indicated by the white arrowheads.

E) Coronal brain image, acquired by the conventional X-ray system. The branches are also clearly visualized, as indicated by the black arrowheads.

F) Coronal brain image, acquired by indirect exposure to the cerium anode X-ray system after a 10-cm-thick acrylic plate was placed between the X-ray system and the brain. The branches are clear, as visualized in Fig. 4 D, and are indicated by the white arrowheads.

G) Coronal brain image, acquired by indirect exposure using the conventional X-ray system with a 10-cm-thick acrylic plate. The branches can be visualized, as indicated by the black arrowhead; however, these structures are difficult to discriminate from one another.

H) Coronal brain image, acquired by indirect exposure to the cerium anode X-ray system with a 20-cm-thick acrylic plate. Although the branches are blurred, as indicated by the white arrowheads, they can still be distinguished.

I) Coronal brain image, acquired by indirect exposure to the conventional X-ray system with a 20-cm-thick acrylic plate. The image is heavily blurred, and the branches are difficult to recognize.

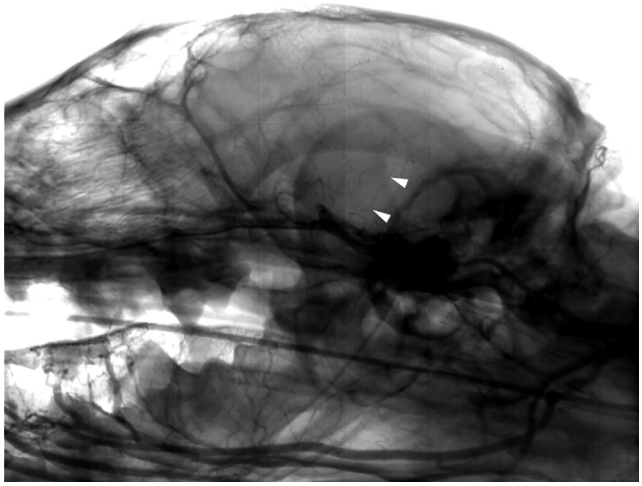

Fig. 5 Image acquired using the cerium anode X-ray system during iodine perfusion in an in-situ dog model. Iodine moving inside the perforating branches from the MCA can be clearly visualized, as indicated by the white arrowheads.

strates clinical potential for visualizing the perforating branches spanning from the MCA.

The spatial resolution of the cerium anode X-ray system compared to conventional X-ray systems

The cerium anode X-ray system featured a detector with a 50 μm resolution, and in the chart study, the empirical resolution was confirmed at 103 μm or less. The perforating branches spanning from the MCA are difficult to analyze using conventional X-ray systems. In clinical settings, angiography is reportedly the best diagnostic tool for the imaging of intracranial vessels, however, the Innova IGS 630 with Innova CT HD (GE health care Japan, Tokyo, Japan), which is used for brain angiography in the authors' institute features a pixel pitch of 200 μm. This is insufficient for visualizing perforating branches from the MCA, because their diameter is sometimes less than 100 μm (Figs. 3, 4, and 5). CT angiography and MR angiography are also commonly used for the evaluation of intracranial vessels. The spatial resolution of a CT scan using Siemens SOMATOM Definition Flash (Siemens Global, Munich, Germany), and an MRI using Ingenia 3.0 T (Philips International B.V., Amsterdam, Netherlands), which are both used for brain angiography in the authors' institute, is 0.39 × 0.39 × 0.75 mm, and 0.65 × 0.65 × 0.70 mm, respectively. According to recent reports, CT digital subtraction angiography using 320-detector row CT features a spatial resolution of 0.5 mm^3 isotropic voxel size [9]. Four-Dimension contrast-enhanced MRI angiography at 3T demonstrates a spatial resolution of 0.9 × 0.9 × 1.5 mm [10]. Additionally, ultra-high resolution MRI at 9.4 T has been used to conduct studies in clinical settings, featuring a voxel size of 0.13 × 0.13 × 0.8 mm^3 [11]. The cerium anode X-ray system demonstrates better spatial resolution than the conventional and the newly developed systems.

Barium contrast material

Barium was used as contrast material for two experiments, the ex-situ mouse and ex-situ dog studies (experiment 2 and 3.1). The K-edge of barium is at 37.4 keV [12–14], which is close to the K-edge of iodine. Therefore, the cerium anode X-ray system with a peak energy of 34.6 keV still features a relatively high photon number at 37.4 keV. Consequently, the cerium anode X-ray system is able to detect tiny amounts of barium in the small vessels branching from the MCA. Barium is never administered via intravenous injection due to its coagulating nature and high viscosity. In the present study, barium was used as a contrast material in the ex-situ experiments, as barium but not iodine remains in the vascular beds for a period in the excised brain, allowing microangiography of the excised brain. Additionally, the brains were excluded immediately after barium perfusion; therefore, the animals were not physiologically affected by the barium materials.

Consideration of the various animal experiments

The current study investigated whether a new angiographic system using a cerium anode could sufficiently visualize perforating branches from the MCA in ex-situ small animals (mice, Fig. 3), ex-situ large animals (dogs, Fig. 4), and in-vivo large animals (dogs, Fig. 5). Clearer visualization of the cerebral perforating branches was obvious in the excised mice than the excised dogs, as indicated in Figs. 3 and 4. The difference in angiographic imaging potential for the cerebral perforating branches between the ex-situ and in-situ dogs indicates that the amount of X-ray exposure time per frame affects the image quality, wherein the images taken from in-situ dogs are of poorer quality than those obtained ex-situ. However, as shown in Fig. 5, the cerium anode X-ray system is capable of visualizing the perforating branches from the MCA in large animals. By increasing the photon number, it will become increasingly possible to visualize the perforating branches of adult humans in the near future.

Feasibility of clinical application

Special techniques are not required to use the cerium anode X-ray system. Moreover, the common contrast materials typically used in clinical settings are also applicable for imaging vessels with the cerium anode X-ray system. In terms of dosimetry, a CT scan of the adult human brain generates a volume CT dose

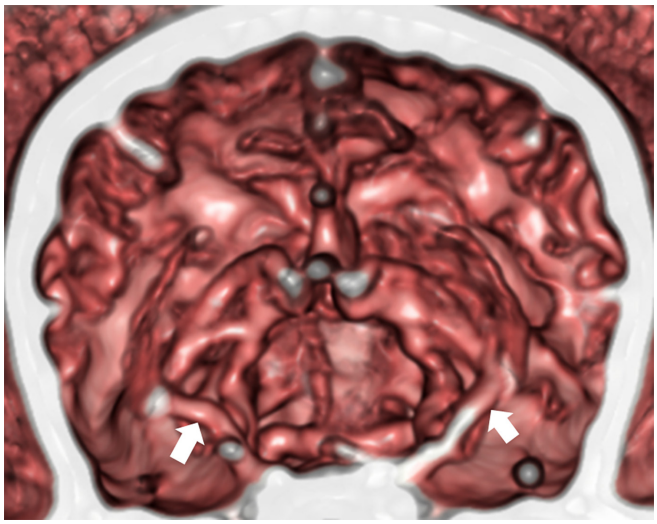

Fig. 6 Image acquired by a CT scan in the same dog. The MCA can be clearly visualized as indicated by the white arrowheads; however, the perforating branches of the MCA are difficult to discriminate.

index of 21.088 mGy (n = 130) using the Siemens SOMATOM Definition Flash, which is used clinically at the authors' institute. By contrast, the use of the cerium anode X-ray system to visualize intracranial microvessels in-situ generated a dosimetry value of 5.34 mGy at 80 kV and 50 mA for 1000 ms at a distance of 50 cm (experiment 1). Therefore, compared to a conventional X-ray system, the dosimetry data for the cerium anode X-ray system seems acceptable. Hence, the cerium anode X-ray system should experience few difficulties in clinical settings.

Future prospects

The cerium anode X-ray system demonstrates the ability to image the perforating branches of the MCA in animals. Our studies suggest that this system could be used for humans, which would lead to the more rapid diagnosis of lacunar strokes in emergencies. Moreover, this system could also be used to help elucidate the arteriovenous malformation in clinical settings. The function of the brain and unknown vascular pathologies may be investigated by the cerium anode X-ray system in the future.

Limitations

The present study features a few potential limitations. First, it is uncertain how useful the cerium anode X-ray system is in actual clinical settings as yet. Second, the cerium anode features a low melting point, which places a limit on both the length and number of exposures.

CONCLUSIONS

In conclusion, the monochromatic X-ray system using a rotating cerium anode is effective in visualizing intracranial microvessels and might be applicable in clinical settings for the early diagnosis of lacunar stroke and other related pathologies.

ACKNOWLEDGMENTS

The study was supported by Grants-in-Aid for Scientific Research B (No.20390336, 2007–2010), Grant-in-Aid for Young Scientists B (No. 25861233, 2013–2014), and Grants-in-Aid from The Cardiovascular Research Fund, Tokyo, Japan (2013–2014). Additionally, it was partly supported by a research grant from Health and Labour Sciences Research Grant (2004–2006) and The Research Funding for Longevity Sciences (22–5) from National Center for Geriatrics and Gerontology (NCGG), Japan.

The authors would like to acknowledge Sachie Tanaka, Yoko Takahari, Yoshiko Shinozaki, and Katsuko Naito (Support Center for Medical Research and Education, Tokai University School of Medicine, Kanagawa, Japan). In addition, we would like to thank Fujio Ando and Rie Hasegawa (Tokai University Imaging Center, Kanagawa, Japan).

REFERENCES

1) Alessandra DB, Palumbo V, Lamassa M, Saia V, Piccardi B, Inzitari D. Progressive lacunar stroke: review of mechanisms, prognostic features, and putative treatments. *Int J Stroke* 2012; 7: 321–329.
2) Behrouz R, Malek AR, Torbey MT. Small vessel cerebrovascular disease: the past, present, and future. *Stroke Res Treat* 2012; 2012: 839151.
3) Dhamoon MS, Mc Clure LA, White CL, Lau H, Benavente O, Elkind MS. Quality of life after lacunar stroke: the secondary prevention of small subcortical strokes study. *J Stroke Cerebrovasc Dis* 2014; 23: 1131–1137.
4) Bailey EL, Smith C, Sudlow CL, Wardlaw JM. Pathology of lacunar ischemic stroke in humans-a systematic review. *Brain Pathol* 2012; 22: 583–591.
5) Mori H, Haruyama S, Shinozaki Y, Okino H, Iida A, Takanashi R, *et al*. New nonradioactive microspheres and more sensitive x-ray fluorescence to measure regional blood flow. *Am J Physiol* 1992; 263: 1946–1957.
6) Mori H, Hyodo K, Tanaka E, Uddin-Mohammed M, Yamakawa A, Shinozaki Y, *et al*. Small-vessel radiography in situ with monochromatic synchrotron radiation. *Radiology* 1996; 201: 173–177.
7) Sato E, Tanaka E, Mori H, Kawai T, Ichimaru T, Sato S, *et al*. Demonstration of enhanced k-edge angiography using a cerium target x-ray generator. *Med Phys* 2004; 31: 3017–3021.
8) Eugene K, Jiangyang Z, Karen H, Nicole EB, Arvind PP. Vascular phenotyping of brain tumors using magnetic resonance microscopy (μMRI). *J Cereb Blood Flow Metab* 2011; 31: 1623–1636.
9) Fujiwara H, Momoshima S, Akiyama T, Kuribayashi S. Whole-brain CT digital subtraction angiography of cerebral dural arteriovenous fistula using 320-detector row CT. *Neuroradiology* 2013; 55: 837–843.
10) Nishimura S, Hirai T, Shigematsu M, Kitajima M, Morioka M, Kai Y, *et al*. Evaluation of brain and head and neck tumors with 4D contrast-enhanced MR angiography at 3T. *AJNR Am J*

Neuroradiol 2012; 33: 445–448.
11) Juliane BG, Shajan KS, Rolf P. Ultra-high resolution imaging of the human brain using acquisition-weighted imaging at 9.4 T. *Neuroimage* 2014; 86: 592–598.
12) Matsukiyo H, Watanabe M, Sato E, Osawa A, Enomoto T, Nagao J, *et al*. X-ray fluorescence camera for imaging of iodine media in vivo. *Radiol Phys Technol* 2009; 2: 46–53.
13) Abudurexiti A, Kameda M, Sato E, Abderyim P, Enomoto T, Watanabe M, *et al*. Demonstration of iodine K-edge imaging by use of an energy-discrimination X-ray computed tomography system with a cadmium telluride detector. *Radiol Phys Technol* 2010; 3: 127–135.
14) Mori H, Hyodo K, Tobita K, Chujo M, Shinozaki Y, Sugishita Y, *et al*. Visualization of penetrating transmural arteries in situ by monochromatic synchrotron radiation. *Circulation* 1994; 89: 863–87.